

Design of drought early warning system based on standard precipitation index prediction using hybrid ARIMA-MLP in Banten Province

Santoso Soekirno¹, Naufal Ananda², Haryas Subyantara Wicaksana², David Yulizar¹,
Muhammad Agung Prabowo¹, Suko Prayitno Adi³, Bayu Santoso²

¹Department of Physics, Faculty of Mathematics and Science, University Indonesia, Depok, Indonesia

²Department of Instrumentation and Control, Faculty of Industrial Technology, Bandung Institute of Technology, Bandung, Indonesia

³Department of Geophysics, State College of Meteorology Climatology and Geophysics, Jakarta, Indonesia

Article Info

Article history:

Received Aug 28, 2023

Revised Nov 8, 2023

Accepted Dec 2, 2023

Keywords:

Autoregressive integrated moving average
Drought
Hybrid
Multi layer perceptron
Standard precipitation index

ABSTRACT

Drought early warning system (DEWS) is an effort to disseminate early warning information based on climate and hydrology aspects. The DEWS design uses autoregressive integrated moving average (ARIMA), multi layer perceptron (MLP), and hybrid ARIMA-MLP models to predict drought based on standard precipitation index (SPI) for 1 month (SPI1), 3 months (SPI3), and 6 months (SPI6). Predictions were made using ERA5 monthly rainfall data from 1981-2022 corrected based on observation data on 9 grids of observation rain gauges in Banten Province. The design of the ARIMA model is determined by selecting the combination of p and q parameters with the lowest Akaike information criterion (AIC) value, while the MLP architecture is determined by referring to the study literature and by trial-and-error testing. ARIMA models and hybrid models are not able to follow actual data fluctuations and have high error values in both SPI1, SPI3, and SPI6, so they are not recommended in this study. The MLP model has the best prediction ability, namely in SPI6 prediction with nash-sutcliffe efficiency (NSE), mean absolute percentage error (MAPE), and root mean square error (RMSE) value.

This is an open access article under the [CC BY-SA](https://creativecommons.org/licenses/by-sa/4.0/) license.



Corresponding Author:

Santoso Soekirno

Department of Physics, Faculty of Mathematics and Science, University Indonesia

Depok, West Java, Indonesia

Email: santoso.s@sci.ui.ac.id

1. INTRODUCTION

El Nino Southern Oscillation (ENSO) variability triggers climate anomalies in Southeast Asia [1]. The tendency of the El Nino phenomenon caused Indonesia to experience a prolonged drought in the April to May period. This disaster is quite detrimental to agriculture due to the reduced water availability for irrigation. The risk of crop failure threatens regional and even national food security [2]. Drought also increases the likelihood of forest and land fires. Based on analysis, the northern part of Banten has a high potential for drought based on rainfall data for 2021-2022 [3]. Drought reduced the productivity of Lebak Regency's rice harvest from 1.65 million tons in 2020 to 1.63 million tons in 2021 [4]. Early information on the possibility of drought should be essential for the quantity of crop harvest in Banten.

The drought early warning system (DEWS) states efforts to disseminate early warning information based on climate and hydrological aspects. Damage indicators can be seen from rainfall parameters, temperature, river discharge, soil moisture, and air supply availability [5]. The accumulation of these indicators

is then expressed numerically in the form of a drought index. The standard precipitation index (SPI) is one of the drought indices calculated through rainfall analysis. This index is used as a DEWS estimator.

Seventy-eight rainfall gauges have been installed in Banten. Monthly rainfall data using the gauges is combined with satellite spatial data to produce spatially corrected total rainfall as an estimator input. SPI is targeted as the DEWS output estimator. Direct measurement at ground stations can improve the quality of SPI data compared to satellite remote sensing.

2. METHOD

Banten is located on the island of Java, Indonesia. The province has an area of 9,662 km². Topographically, Banten is in a lowland area with an average elevation of 258 m [4]. This study focuses on Banten at latitude 6.000 S-6.750 S and longitude 105.500 E-106.250 E. There are 30 obs rain gauges. These instruments work based on manual volumetric measurements using obs glass. The obs rain gauges are verified and calibrated regularly every year. Obs rain gauges validate remote sensing-based rainfall measurements such as radar and weather satellites [6]. Table 1 shows the location of the obs rain gauges and the coordinate grid based on the focus of the study area.

Table 1. Location of obs rain gauge and grid satellite

Grid	Satellite		Regency	Obs rain gauge			Distance to grid (km)
	Lat	Lon		Site	Lat	Lon	
6	-6.25	105.75	Pandeglang	Jiput	-6.349	105.866	16.90
			Pandeglang	Mekarjaya	-6.504	105.815	7.17
			Pandeglang	Sobang	-6.560	105.770	9.18
7	-6.5	105.75	Pandeglang	Pagelaran	-6.432	105.859	13.26
			Pandeglang	Cigeulis	-6.550	105.640	13.33
			Pandeglang	Labuhan	-6.379	105.832	15.25
			Pandeglang	Munjul	-6.609	105.871	18.52
			Pandeglang	Cibaliung	-6.716	105.706	6.42
8	-6.75	105.75	Pandeglang	Nanggala	-6.736	105.841	10.21
			Pandeglang	Cikeusik	-6.725	105.873	13.98
			Pandeglang	Cimanggu	-6.660	105.640	15.59
9	-6	106	Cilegon	Cigeblang	-6.020	105.980	2.79
			Cilegon	Pulo Merak	-5.960	106.010	5.61
			Cilegon	Cilegon	-6.017	106.067	7.72
			Pandeglang	Pulosari	-6.341	105.937	12.01
			Pandeglang	Cimanuk	-6.350	106.044	12.05
10	-6.25	106	Pandeglang	Bunut	-6.270	106.110	12.35
			Pandeglang	Mandalawangi	-6.311	105.906	12.37
			Pandeglang	Cipeucang	-6.362	106.027	12.97
			Pandeglang	Pandeglang	-6.311	106.106	13.48
			Pandeglang	Menes	-6.377	105.920	16.27
11	-6.5	106	Pandeglang	Cilemer	-6.494	106.015	1.90
			Pandeglang	Bojong	-6.471	106.000	3.19
12	-6.75	106	Pandeglang	Ciliman	-6.640	105.990	11.97
			13	-6	106.25	Serang	Kasemen
14	-6.25	106.25	Serang			Curug	-6.190
			Serang	Walantaka	-6.147	106.232	11.16
			Pandeglang	Cisangu	-6.310	106.140	13.83
			Serang	Cipari	-6.135	106.200	14.10
			Serang	Tengkile	-6.135	106.164	15.87

Table 1 shows the locations of rain gauges and grid data obtained from ERA5 satellite data. ERA5 is the fifth generation of the European Centre for Medium-Range Weather Forecasts (ECMWF) reanalysis data as a product of the Copernicus program. ERA5 measurement parameters are uploaded in Copernicus climate data store (CCDS). CCDS is one of the copernicus climate change service (C3S) subprogram outputs [7]. ERA5 integrates various satellite data products in the integrated forecasting system (IFS). ERA5 data has a spatial resolution of 31 km or a grid resolution of 0,25° [8]. Obs rain gauge data and ERA5 data were taken for 1981-2022. SPI analysis requires climatological data with a minimum period of 30 years. Obs daily rainfall data is processed into monthly rainfall data. Meanwhile, ERA5 data is the total monthly rainfall.

Figure 1 shows the flow of the system running in this study, starting with preprocessing. Pre-processing of obs rain gauge data is done through a range check. Daily rainfall data does not exceed 508 mm [9]. Out-of-range data were considered outliers and removed. The ERA5 data was verified against the obs resample data according to the grid in Table 1. This verification resulted in the following bias factor (B(x)) values [10].

$$B(x) = \frac{\sum_{i=1}^n R(x_i)}{\sum_{i=1}^n S(x_i)}$$

$R(x_i)$ is obs rain gauge data, while $S(x_i)$ is satellite data. If the number of rain gauges is more than one, then the bias factor value is weighted. The weighting is calculated based on the distance of the obs rain gauge to the nearest grid. The weighting equation uses the inverse distance weighting (IDW). $W(x)$ is the weighting of one obs rain gauge. $D(x,y)$ represents the distance of the rain gauge coordinates to the satellite grid coordinates. Multisite obs rain gauge bias factor results ($B(x)$) obtained as [10]:

$$B_m(x) = \frac{\sum_{i=0}^n W_i(x) \cdot B_i(x)}{\sum_{i=0}^n W_i(x)} = \frac{\sum_{i=0}^n \frac{B_i(x)}{D_i^2(x,y)}}{\sum_{i=0}^n \frac{1}{D_i^2(x,y)}}$$

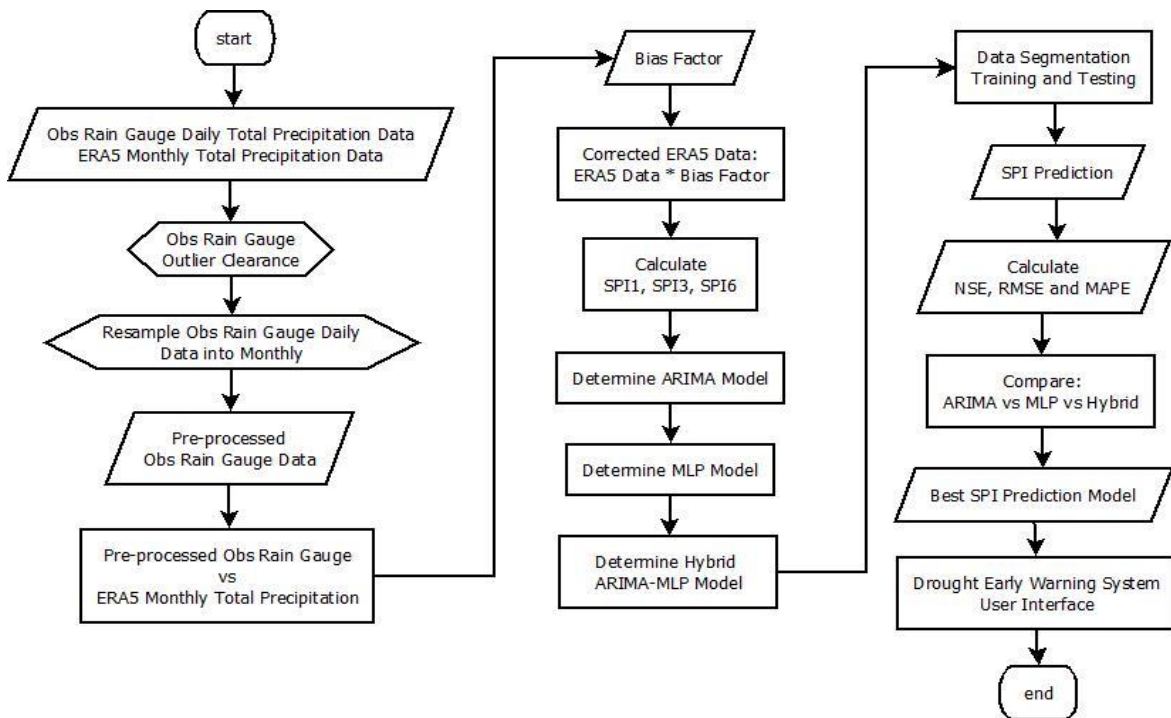


Figure 1. Flowchart DEWS in this research

Corrected satellite data results from multiplying the ERA5 data by the bias factor value. This data is then further processed into SPI values. The SPI calculation requires total monthly rainfall data. SPI expresses a drought index based on long-term precipitation data. The rainfall data is adjusted to the Gamma distribution and then converted to a normal distribution [11]. The Gamma distribution is highly compatible with sequential periods of rainfall data [12]. The Gamma distribution probability function equation is expressed as:

$$g(x) = \frac{1}{\beta^\alpha \Gamma(\alpha)} x^{\alpha-1} e^{-x/\beta}$$

β , α , x dan $\Gamma(\alpha)$ represent scale, shape variables, total rainfall, and Gamma function, respectively. The parameters β dan α need to be estimated to model the Gamma probability distribution function [13]. The estimation of both parameters can be calculated using Thom's approximation [11].

$$\alpha = \frac{1}{4A} \left[1 + \sqrt{1 + \frac{4A}{3}} \right]; \beta = \frac{\bar{x}}{\alpha}; A = \ln(\bar{x}) - \frac{\sum \ln(x)}{n}$$

After estimating β dan α , fungsi $g(x)$ function is used to obtain the cumulative probability function $G(x)$. This function is expressed as:

$$G(x) = \int_0^\infty g(x) dx = \frac{1}{\beta\alpha\tau(\alpha)} \int_0^x x^{\alpha-1} e^{-x/\beta} dx = \frac{1}{\tau(\alpha)} \int_0^x t^{\alpha-1} e^{-t} dt$$

If there is a possibility that rain does not occur, then the $G(x)$ function needs to be corrected. If q is the probability of no rain, then the cumulative probability function becomes:

$$H(x) = q + (1 - q)G(x)$$

Equation $H(x)$ is then transformed into a standardized normal distribution. The result of this transformation shows the SPI value. The SPI formulation is expressed as:

$$SPI = - \left[t - \frac{c_0 + c_1 t + c_2 t^2}{1 + d_1 t + d_2 t^2 + d_3 t^3} \right], t = \sqrt{\ln \left[\frac{1}{(H(x))^2} \right]}, \text{ untuk } 0 < H(x) < 0.5$$

$$SPI = + \left[t - \frac{c_0 + c_1 t + c_2 t^2}{1 + d_1 t + d_2 t^2 + d_3 t^3} \right], t = \sqrt{\ln \left[\frac{1}{(1-H(x))^2} \right]}, \text{ untuk } 0.5 < H(x) < 1$$

The index is adaptive to seasonal zone variations and explains rainfall deficits thoroughly. World Meteorological Organization uses SPI as a drought monitoring tool [5]. Table 2 shows the physical meaning of SPI values as a drought index.

Table 2. Index of SPI and type of drought

Range of SPI	Type of drought	Range of SPI	Type of drought
≥ 2.0	Extreme wet	$-1.49 \leq SPI \leq -1.0$	Moderate drought
$1.5 \leq SPI \leq 1.99$	Very wet	$-1.99 \leq SPI \leq -1.5$	Severe drought
$1.0 \leq SPI \leq 1.49$	Moderate wet	≤ -2.0	Extreme drought
$-0.99 \leq SPI \leq 0.99$	Normal		

SPI forecasts drought in 1 month (SPI1), 3 months (SPI3), 6 months (SPI6), 9 months (SPI9), and 12 months (SPI12). The 3-month forecast is capable of monitoring drought. The 6-month forecast can analyze the impact of drought on agriculture [14]. The hybrid autoregressive integrated moving average (ARIMA)-multi layer perceptron (MLP) model is a model that solves linear and nonlinear problems sequentially. The ARIMA model estimates the air temperature linearly. The ARIMA residuals contain a nonlinear model. If y_t is actual value dan \hat{L}_t is the estimated value of ARIMA, then the residual value (e_t) is mathematically expressed as [15]:

$$e_t = y_t - \hat{L}_t$$

The nonlinear model is then estimated using the MLP algorithm. If \hat{N}_t is the MLP estimate and b is the MLP bias, the residual value relationship (e_t when expressed in MLP, the nonlinear function is described as:

$$\hat{N}_t = f(e_{t-1}, e_{t-2}, \dots, e_{t-n}) + b$$

Furthermore, the combination of ARIMA and MLP estimates is summed up to produce the final estimation value of the hybrid model. The hybrid model estimation equation is expressed as [16]:

$$\hat{y}_t = \hat{L}_t + \hat{N}_t$$

The accuracy of the output prediction results and testing of ARIMA, MLP, and hybrid ARIMA-MLP models is evaluated using nash-sutcliffe efficiency (NSE), root mean square error (RMSE), and mean absolute percentage error (MAPE). These three parameters are standard for analyzing drought index prediction models [17].

3. RESULTS AND DISCUSSION

3.1. Corrected ERA5 data pre-processing result

Drought prediction, a challenge for researchers, still has room for improvement in hybrid technique models [18]. This research was conducted by designing ARIMA, MLP, and hybrid ARIMA-MLP algorithms to find the best SPI prediction design in DEWS in Banten Province. Rainfall data obtained from the ERA5

satellite was verified against obs rain gauge data from 1981-2022. SPI predictions using ARIMA, MLP, and hybrid ARIMA-MLP algorithms were designed using ERA5 data from 1981 to 2013. The SPI ARIMA, MLP, and hybrid ARIMA-MLP prediction models were tested by verifying SPI prediction data against actual SPI data in 2014-2022. Pre-processing was implemented on the ERA5 data to obtain corrected data based on direct measurements by obs rain gauges. Monthly rainfall data from ERA5 was compared to monthly obs rain gauge data according to the nearest grid coordinates for 1981-2022. The comparison resulted in a bias factor value per ERA5 grid. The bias factor serves to correct the ERA5 rainfall data. Furthermore, the corrected data is evaluated against the initial data using the correlation, RMSE, and MAPE parameters. Table 3 shows the bias factor of the ERA5 rainfall parameter data against the obs rain gauge.

Table 3 shows the results of the verification of ERA5 data that has been corrected with bias factors in the form of correlation, RMSE, and MAPE against rain gauge data on grids 6-14. Correlation or correlation coefficient shows how well the predicted quantity correlates or relates to the observed quantity and displays the extent to which the two variables are directly related. A correlation value of 0.0-0.2 indicates a very weak relationship, 0.2-0.4 is weak, 0.4-0.6 is moderate, 0.6-0.8 is strong, and 0.8-1.0 is very strong. RMSE is the standard deviation of the model's predicted results, which indicates how closely the forecast matches the observations [19]. MAPE is the average absolute error percentage. The model's ability will be better with a smaller RMSE value, which indicates a small error value and a more significant correlation value [20].

Table 3. Bias factor, correlation, uncorrected, corrected, RMSE and MAPE ERA5 data pre-processing

Grid	Bias factor	Rain gauge	Correlation	RMSE (mm)		MAPE (%)	
				Uncorrected	Corrected	Uncorrected	Corrected
6	1.39	Jiput	0.63	192.75	192.40	84.15	56.35
		Mekarjaya	0.79	121.27	117.18	62.01	50.81
		Sobang	0.75	145.91	136.17	72.76	57.80
7	1.20	Pagelaran	0.70	132.16	162.87	60.06	57.83
		Cigeulis	0.77	201.44	176.07	66.60	49.42
		Labuhan	0.78	125.76	130.02	61.58	52.56
		Munjul	0.80	159.83	146.89	67.49	54.58
8	1.21	Cibaliung	0.82	151.09	135.89	67.66	54.04
		Nanggala	0.87	102.19	99.84	55.56	47.96
		Cikeusik	0.61	188.43	203.95	69.10	61.66
		Cimanggu	0.73	162.90	163.05	60.18	51.88
9	1.21	Cigeblang	0.55	215.63	205.99	64.00	56.08
		Pulo Merak	0.74	91.15	104.58	42.43	45.68
		Cilegon	0.61	184.58	175.71	60.12	52.77
		Pulosari	0.76	228.13	200.70	80.17	62.41
10	1.17	Cimanuk	0.66	131.67	137.10	46.59	43.20
		Bunut	0.60	112.62	125.96	56.85	49.31
		Mandalawangi	0.64	185.06	181.82	56.69	49.79
		Cipeucang	0.67	143.08	153.21	51.84	50.34
11	0.76	Pandeglang	0.51	193.69	188.99	66.74	56.48
		Menes	0.77	153.35	139.58	53.11	44.86
		Cilemer	0.71	137.45	121.91	47.08	49.44
		Bojong	0.54	222.59	213.10	63.43	73.34
12	0.73	Ciliman	0.71	126.24	108.87	49.84	54.21
		Kasemen	0.68	108.97	63.56	56.54	57.45
13	0.48	Curug	0.80	78.38	76.31	47.46	51.26
		Walantaka	0.65	111.10	102.33	49.43	49.36
		Cisangu	0.53	129.11	129.90	75.74	83.60
14	0.92	Cipari	0.68	106.32	94.09	45.44	45.04
		Tengkile	0.69	109.47	100.08	47.44	46.68

Remote sensing-based rainfall measurements are biased due to evaporation factors and wind movement before reaching the earth's surface. After obtaining the bias-factor value, corrections were made to the ERA5 data. Then, the calculation and comparison of RMSE and MAPE of uncorrected and corrected ERA5 data against ARG observation data can be seen in Table 3. Applying the bias factor can improve the accuracy of ERA5 rainfall data. This is evidenced by decreased RMSE and MAPE values against obs rain gauges in several grids after correction. Based on the correlation value of the ERA5 model with observations in Table 3, it is known that the ability of corrected-ERA5 is competent in modeling rainfall data at the observation point. Most of the correlations are >0.6 , which indicates a strong relationship where the model can follow the fluctuations of the actual conditions [21]. The distance of the gauge to the grid and the density of the gauge significantly affects the accuracy of the correction results. The closer the distance to the grid point, the better the correlation between the two data. The denser the number of gauges in one grid, the lower the RMSE and

MAPE values. The corrected-ERA5 data is used to calculate SPI values of SPI1, SPI3, and SPI6 in the period 1981-2022. The SPI data is used to design ARIMA, MLP, and hybrid algorithms. ARIMA models are divided into autoregressive (AR), moving average (MA), and autoregressive moving average (ARIMA) models. The ARIMA model has no differentiation process, so the parameter value $d=0$, and the ARIMA equation is $(p, 0, q)$ [22]. Table 4 shows the results of the ARIMA model design.

Table 4 is an ARIMA model design using a combination of p , d , and q parameters based on auto-correlation function (ACF), partial auto-correlation function (PACF), and Akaike information criterion (AIC) values. An ARIMA model is built with different combinations. Each combination is calculated for its AIC value, and the optimal combination that produces the lowest AIC value is chosen [23]. Table 4 shows the optimal design of the selected ARIMA (p, q) model on grids 6-15 and the AIC value of each model for SPI1, SPI3, and SPI6. The MLP design in this study is using feed-forward MLP. The feed-forward method is commonly used in drought prediction and hydrology for flooding [24]. The architecture for MLP is determined by referring to previous literature and by trial-and-error testing because no guaranteed MLP architecture can be applied to all predictions [25]. The best structure in this study obtained from testing is 45 hidden neurons. The activation function used is hyperbolic tangential function optimized by the Adam optimizer method. MLP input uses SPI at $t-1$ and $t-2$ [26].

Table 4. Result SPI1, SPI3, and SPI6 of ARIMA model design

Grid	SPI1		SPI3		SPI6	
	Model	AIC	Model	AIC	Model	AIC
6	ARIMA (2,1)	1317.22	ARIMA (1,2)	829.73	ARIMA (2,5)	447.64
7	ARIMA (2,1)	1366.89	ARIMA (2,2)	879.91	ARIMA (1,5)	494.84
8	ARIMA (1,2)	1388.29	ARIMA (2,4)	914.36	ARIMA (4,5)	569.65
9	ARIMA (1,1)	1372.95	ARIMA (1,2)	869.66	ARIMA (2,5)	357.65
10	ARIMA (1,1)	1388.18	ARIMA (1,2)	893.97	ARIMA (2,5)	431.87
11	ARIMA (1,1)	1406.82	ARIMA (5,4)	922.15	ARIMA (1,5)	459.87
12	ARIMA (2,1)	1373.02	ARIMA (5,3)	889.31	ARIMA (1,5)	485.64
13	ARIMA (1,1)	1375.74	ARIMA (1,2)	880.23	ARIMA (1,5)	339.50
14	ARIMA (1,1)	1382.33	ARIMA (1,2)	871.51	ARIMA (2,5)	357.25

3.2. Prediction performance test of SPI1, SPI3, and SPI6

Graphs of predicted and observed values are shown in Figure 2 for SPI1, SPI3, and SPI6. The red line shows the predicted value of the hybrid model, the black line is the MLP model, the yellow line is the ARIMA model, and the blue line is the actual observed value. Figure 2(a) shows that the prediction of SPI in grids 6 of the ARIMA model, MLP model, and hybrid model is not able to follow the actual SPI value fluctuations where there is a clear gap between the graphs of the ARIMA, MLP, and hybrid models against the actual graph. Figure 2(b) shows the MLP model's ability to improve SPI3 prediction significantly. MLP model SPI3 predictions can follow the peak and valley fluctuations of actual values even though there is still an insignificant gap between the MLP model graph and the actual graph [17]. On the other hand, Figure 2(b) shows that the SPI3 prediction ability of the ARIMA and hybrid models is worse than the SPI1 prediction. The gap between the ARIMA and hybrid model graphs and the actual graph is increasingly tenuous and visible. The NSE value of SPI3 prediction of both ARIMA and hybrid models increased from SPI1, but their RMSE and MAPE values also increased significantly.

Figure 2(c) shows that the SPI6 prediction for the MLP model is more accurate than the SPI3 prediction. In Figure 2(c), it can be seen that the gap between the MLP model graph and the actual graph is getting tighter than seen in Figure 2(b), which is in line with the increase in the NSE value and the decrease in the RMSE and MAPE values. However, the ARIMA and hybrid models can still not follow the fluctuations in the actual SPI value, whereas, in the SPI6 prediction plot graph in Figure 2(c), the gap between the ARIMA and hybrid model graphs and the actual graph can still be seen. Adding a period in SPI6 does not improve the prediction ability of ARIMA and hybrid models.

Table 5 verifies SPI1, SPI3, and SPI6 prediction performance tests using ARIMA, MLP, and hybrid ARIMA-MLP models. The verification parameters used are NSE, RMSE, and MAPE. The NSE method is commonly used in hydrological simulations and in testing the effects of model simulations in studying the relationships between climate and hydrological processes [23]. NSE is the ratio of mean square error and variance, which shows the closeness of the relationship between observed data and simulated data. A perfect model will be the same as the observation, and the value of $NSE=1$ indicates this perfection.

Table 5 shows that the NSE value of the ARIMA model ranges from -0.11 to 0.08, while the MLP model is -0.21 to 0.06, and the hybrid model is -1.46 to -0.82. The RMSE and MAPE values of the ARIMA model range from 1.02 to 1.19 and 8.43 to 9.55, while the MLP model is 0.84 to 0.97 and 7.02 to 7.87, and the hybrid model is 1.04 to 1.19 and 8.67 to 9.97. The ability of the SPI1 prediction model for all grids still needs

to be more competent based on the RMSE value, which reaches even more than 1, and the small NSE even reaches a minus value.

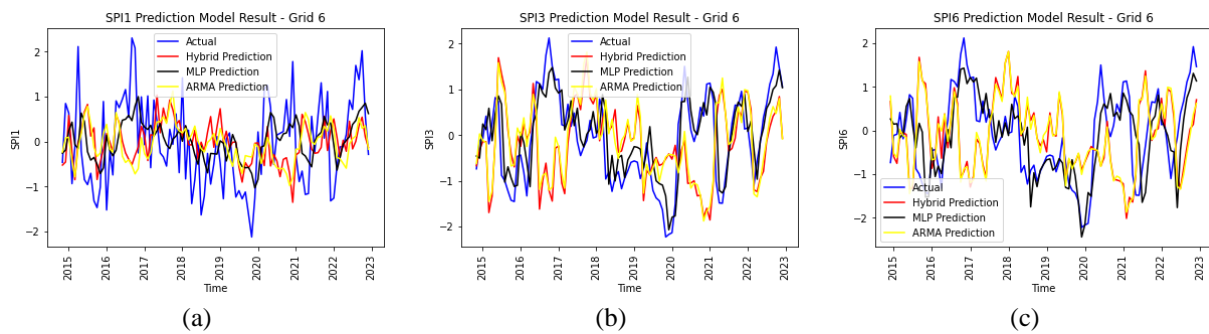


Figure 2. Prediction plot results of (a) SPI1, (b) SPI3, and (c) SPI6

Table 5. SPI1, SPI3 and SPI6 prediction performance test results

Grid	Error Metric	SPI1			SPI3			SPI6		
		ARIMA	MLP	Hybrid	ARIMA	MLP	Hybrid	ARIMA	MLP	Hybrid
6	NSE	-0.04	-0.12	-0.95	0.69	0.47	-0.88	0.82	0.52	-0.99
	RMSE	1.06	0.87	1.08	1.26	0.54	1.33	1.27	0.46	1.37
	MAPE	8.69	7.33	9.09	10.35	4.15	11.49	10.47	3.76	11.68
7	NSE	-0.06	-0.10	-0.95	0.66	0.48	-0.70	0.77	0.52	-0.98
	RMSE	1.10	0.92	1.13	1.30	0.58	1.32	1.31	0.51	1.42
	MAPE	9.11	7.62	9.51	10.76	4.61	11.40	10.89	4.10	12.15
8	NSE	-0.08	-0.19	-0.90	0.66	0.49	-0.66	0.77	0.44	-0.89
	RMSE	1.16	0.97	1.19	1.35	0.60	1.35	1.36	0.55	1.44
	MAPE	9.55	7.87	9.97	11.13	4.89	11.26	11.26	4.26	12.27
9	NSE	0.05	0.05	-0.83	0.74	0.59	-0.70	0.90	0.76	-0.79
	RMSE	1.02	0.84	1.04	1.30	0.53	1.33	1.43	0.42	1.37
	MAPE	8.43	7.02	8.67	10.61	4.29	11.04	11.56	3.44	11.54
10	NSE	-0.01	-0.02	-1.46	0.72	0.52	-0.62	0.88	0.66	-0.86
	RMSE	1.07	0.89	1.18	1.37	0.57	1.38	1.49	0.46	1.48
	MAPE	8.94	7.74	10.05	11.38	4.68	11.98	12.42	3.94	12.76
11	NSE	-0.11	-0.21	-1.42	0.67	0.50	-0.66	0.87	0.63	-0.96
	RMSE	1.07	0.92	1.12	1.36	0.60	1.38	1.45	0.47	1.51
	MAPE	8.81	7.83	9.55	11.28	4.81	11.84	12.05	4.03	13.03
12	NSE	-0.11	-0.20	-0.97	0.66	0.51	-0.68	0.82	0.59	-0.96
	RMSE	1.11	0.95	1.16	1.36	0.62	1.38	1.40	0.51	1.49
	MAPE	9.11	7.82	9.89	11.28	4.83	12.01	11.63	4.02	12.97
13	NSE	0.04	0.02	-0.96	0.73	0.54	-0.75	0.91	0.63	-0.74
	RMSE	1.05	0.86	1.11	1.31	0.55	1.36	1.43	0.41	1.36
	MAPE	8.67	7.14	9.34	10.69	4.48	11.20	11.55	3.37	11.58
14	NSE	0.08	0.06	-0.82	0.72	0.54	-0.63	0.90	0.67	-0.87
	RMSE	1.05	0.87	1.12	1.32	0.57	1.32	1.43	0.42	1.42
	MAPE	8.77	7.41	9.47	10.82	4.71	11.44	11.68	3.56	11.89

In Table 5, the NSE values of the ARIMA model range from 0.66 to 0.74, while the hybrid model is -0.88 to -0.62. The RMSE and MAPE values of the ARIMA model range from 1.26 to 1.37 and 10.35 to 11.38, while the hybrid model is 1.32 to 1.38 and 11.04 to 11.98. The NSE value of SPI6 prediction of the MLP model ranged from 0.44 to 0.67, with RMSE and MAPE values between 0.41 to 0.55 and 3.37 to 4.26. Most of the MLP model's SPI6 prediction NSE values are >0.5, which states that the model is acceptable and neither over-estimated nor under-estimated. The fluctuation of the NSE value of the hybrid model on all grids is not related to the increase in the period that the NSE value of the hybrid model increases at SPI3 against SPI1 and decreases at SPI6 against SPI3. The RMSE and MAPE values of the Hybrid model also increased from SPI1 to SPI6.

The NSE value of the SPI6 prediction of the ARIMA model increased to almost 1, but the RMSE and MAPE values were also significant, so the model's ability did not increase. The NSE value of the ARIMA model ranges from 0.77 to 0.91, while the hybrid model is -0.99 to -0.74. The RMSE and MAPE values of the ARIMA model range from 1.27 to 1.49 and 10.47 to 12.42, while the hybrid model is 1.36 to 1.51 and 11.54 to 13.03, which can be seen in Table 5. The distance from the prediction value line of the ARIMA and hybrid models to the actual value line is increasingly stretched as the period increases, namely from SPI1, SPI3, and

SPI6. At the same time, the distance from the MLP model prediction value line to the actual value line is getting closer as the time range increases, namely from SPI1, SPI3, and SPI6. The hybrid model has a pattern similar to the ARIMA model. The MLP model shows the pattern that best follows the actual observations in the SPI6 prediction.

3.3. Discussion

Figures 2(a)-(c), show that the SPI1 graph fluctuates more than the SPI3 graph, and the SPI3 graph fluctuates more than the SPI6 graph. This is because predictions for a smaller period can respond to small changes in precipitation and thus capture more monthly droughts than longer spans. Therefore, predictions with extended time spans can also be more accurate because they fluctuate less. Based on Figures 2(a)-(c) and Table 5, it can be seen that as the period increases, the ability to predict SPI using the ARIMA model and the MLP model increases, indicated by the NSE value, which is getting more significant near the value of 1. However, the ARIMA model's RMSE and MAPE values increase as the SPI prediction period increases, reducing the model's ability.

This study does not recommend the hybrid model because it has a low NSE value and high RMSE and MAPE values. The hybrid model is a combination of ARIMA and MLP single models. Hence, factors that affect the increase or decrease in the ability of each single model also affect the hybrid model. The increase in errors in the ARIMA model as the prediction period increases also causes an increase in errors in the hybrid model as the prediction period increases. Figures 2(a)-(c) show that the hybrid model has a similar pattern to the ARIMA model pattern. The ARIMA and hybrid models' graphs are close together and almost overlap for both SPI1, SPI3, and SPI6 predictions. On the other hand, the ARIMA model does have a high NSE value, but its RMSE and MAPE values are more significant than the MLP model. The MLP model is the most competent compared to the other two models in predicting SPI based on its RMSE, MAPE, and NSE values. This supports several previous studies showing that the MLP model has better SPI simulation capabilities than ARIMA and other models. With low RMSE and MAPE values reaching 0.6, the MLP model in SPI6 prediction is the best design compared to other prediction models.

During 2018-2020, most areas of Banten Province experienced moderate to severe drought. Moderate drought occurred in 2018 and 2019. Meanwhile, extreme drought occurred in late 2019 to early 2020. This is confirmed by the decline in productivity of food and horticultural crops in Banten since 2018 [4]. This information can be predicted by the MLP model based on SPI3 and SPI6 parameters in Figures 2(b) and (c). The MLP model as an estimator of SPI3 and SPI6 can potentially become an algorithm for developing the DEWS.

4. CONCLUSION

ARIMA, MLP, and hybrid ARIMA-MLP models were used to predict SPI at 9 grid locations in Banten Province. SPI predictions were made for 1, 3, and 6 months using ERA5 monthly precipitation data corrected based on rain gauge observation data. The ARIMA model design was determined by selecting the combination of p and q parameters with the lowest AIC value. MLP architecture is determined by referring to previous literature and trial and error testing. The hybrid model is a combination of ARIMA and MLP estimates summed to produce the final estimated value of the hybrid model. The results show that the ARIMA model is similar to the hybrid model seen from the graph and the error value. This study does not recommend the ARIMA and hybrid models because they have high error values, namely the RMSE and MAPE values that reach >1 both in SPI1, SPI3, and SPI6 even though the NSE value in SPI6 is high, reaching 1. This study recommends the MLP model with the best prediction ability, namely in SPI6 prediction. This research is expected to be a reference and consideration for developing SPI-based DEWS in Banten Province.

ACKNOWLEDGEMENTS

All authors acknowledge Universitas Indonesia and Hibah PUTI PASCA SARJANA (Number: NKB-234/UN2.RST/HKP/05.00/2023) for support. We would like to express our gratitude to Indonesia Endowment Fund for Education or Lembaga Pengelola Dana Pendidikan (LPDP) for partially supporting this study and Region II of Indonesia Agency for Meteorology Climatology and Geophysics.




REFERENCES

- [1] R. V. Rohli and A. J. Vega, *Climatology*, Burlington, Vermont: Jones & Bartlett Learning, 2018.
- [2] BMKG, *Climate outlook 2023*. Jakarta: BMKG, 2022.
- [3] BNPB (2021) 'National Disaster Risk Study in Banten Province 2022 - 2026', Deputy for Systems and Strategy, Directorate of Disaster Risk Mapping and Evaluation, p. 173.
- [4] "Banten province in 2022 (in Indonesian: Provinsi Banten dalam angka 2022)," *BPS Banten*, 2022. [Online]. Available:




- <https://banten.bps.go.id/publication/2022/02/25/19658ae14140f17fc6ae9e3a/provinsi-banten-dalam-angka-2022.html>. Access date: 10 September 2023
- [5] Global Water Partnership and World Meteorological Organization, *Handbook of drought indicators and indices*. Lincoln, Nebraska: Integrated Drought Management Programme, 2016.
 - [6] R. Hambali, D. Legono, and R. Jayadi, "Correcting radar rainfall estimates based on ground elevation function," *Journal of the Civil Engineering Forum*, vol. 5, no. 3, pp. 301-310, Sep. 2019, doi: 10.22146/jcef.49395.
 - [7] N. Oses, I. Azpiroz, S. Marchi, D. Guidotti, M. Quartulli, and I. G. Olaizola, "Analysis of Copernicus' ERA5 climate reanalysis data as a replacement for weather station temperature measurements in machine learning models for olive phenology phase prediction," *Sensors*, vol. 20, no. 21, pp. 1-22, Nov. 2020, doi: 10.3390/s20216381.
 - [8] H. Hersbach *et al.*, "The ERA5 global reanalysis," *Quarterly Journal of the Royal Meteorological Society*, vol. 146, no. 730, pp. 1999-2049, Jul. 2020, doi: 10.1002/qj.3803.
 - [9] C. A. Fiebrich, C. R. Morgan, A. G. McCombs, P. K. Hall, and R. A. McPherson, "Quality assurance procedures for mesoscale meteorological data," *Journal of Atmospheric and Oceanic Technology*, vol. 27, no. 10, pp. 1565-1582, Oct. 2010, doi: 10.1175/2010JTECHA1433.1.
 - [10] K. Tesfagiorgis, S. E. Mahani, N. Y. Krakauer, and R. Khanbilvardi, "Bias correction of satellite rainfall estimates using a radar-gauge product-a case study in Oklahoma (USA)," *Hydrology and Earth System Sciences*, vol. 15, no. 8, pp. 2631-2647, Aug. 2011, doi: 10.5194/hess-15-2631-2011.
 - [11] T. B. McKee, N. J. Doesken, and J. Kleist, "Drought monitoring with multiple time scales," in *Proceedings of the 9th Conference on Applied Climatology*, pp. 233-236, 1995.
 - [12] Y. Zhang, H. Yang, H. Cui, and Q. Chen, "Comparison of the Ability of ARIMA, WNN and SVM models for drought forecasting in the Sanjiang plain, China," *Natural Resources Research*, vol. 29, no. 2, pp. 1447-1464, Apr. 2020, doi: 10.1007/s11053-019-09512-6.
 - [13] A. Jalalkamali, M. Moradi, and N. Moradi, "Application of several artificial intelligence models and ARIMAX model for forecasting drought using the standardized precipitation index," *International Journal of Environmental Science and Technology*, vol. 12, no. 4, pp. 1201-1210, Apr. 2015, doi: 10.1007/s13762-014-0717-6.
 - [14] G. Tsakiris and H. Vangelis, "Towards a drought watch system based on spatial SPI," *Water Resources Management*, vol. 18, no. 1, pp. 1-12, Feb. 2004, doi: 10.1023/B:WARM.0000015410.47014.a4.
 - [15] A. Parasyris, G. Alexandrakis, G. V. Kozyrakis, K. Spanoudaki, and N. A. Kampanis, "Predicting meteorological variables on local level with SARIMA, LSTM and hybrid techniques," *Atmosphere*, vol. 13, no. 6, pp. 1-21, May 2022, doi: 10.3390/atmos13060878.
 - [16] D. Xu, Q. Zhang, Y. Ding, and D. Zhang, "Application of a hybrid ARIMA-LSTM model based on the SPEI for drought forecasting," *Environmental Science and Pollution Research*, vol. 29, no. 3, pp. 4128-4144, Jan. 2022, doi: 10.1007/s11356-021-15325-z.
 - [17] K. F. Fung, Y. F. Huang, C. H. Koo, and Y. W. Soh, "Drought forecasting: A review of modelling approaches 2007-2017," *Journal of Water and Climate Change*, vol. 11, no. 3, pp. 771-799, Sep. 2020, doi: 10.2166/wcc.2019.236.
 - [18] M. A. Alawsi, S. L. Zubaidi, N. S. S. Al-Bdairi, N. Al-Ansari, and K. Hashim, "Drought forecasting: a review and assessment of the hybrid techniques and data pre-processing," *Hydrology*, vol. 9, no. 7, pp. 1-23, Jun. 2022, doi: 10.3390/hydrology9070115.
 - [19] M. M. H. Khan, N. S. Muhammad, and A. El-Shafie, "Wavelet based hybrid ANN-ARIMA models for meteorological drought forecasting," *Journal of Hydrology*, vol. 590, Nov. 2020, doi: 10.1016/j.jhydrol.2020.125380.
 - [20] X. Wu *et al.*, "The development of a hybrid wavelet-ARIMA-LSTM model for precipitation amounts and drought analysis," *Atmosphere*, vol. 12, no. 1, pp. 1-17, Jan. 2021, doi: 10.3390/atmos12010074.
 - [21] K. Achour, M. Meddi, A. Zeroual, S. Bouabdelli, P. Maccioni, and T. Moramarco, "Spatio-temporal analysis and forecasting of drought in the plains of northwestern Algeria using the standardized precipitation index," *Journal of Earth System Science*, vol. 129, no. 1, Dec. 2020, doi: 10.1007/s12040-019-1306-3.
 - [22] V. Coban, E. Guler, T. Kilic, and S. Y. Kandemir, "Precipitation forecasting in Marmara region of Turkey," *Arabian Journal of Geosciences*, vol. 14, no. 2, Jan. 2021, doi: 10.1007/s12517-020-06363-x.
 - [23] M. Alquraish, K. Ali. Abuhasel, A. S. Alqahtani, and M. Khadr, "SPI-based hybrid hidden Markov-GA, ARIMA-GA, and ARIMA-GA-ANN models for meteorological drought forecasting," *Sustainability*, vol. 13, no. 22, pp. 1-24, Nov. 2021, doi: 10.3390/su132212576.
 - [24] D. Hong and K. A. Hong, "Drought forecasting using MLP neural networks," in *2015 8th International Conference on u- and e-Service, Science and Technology (UNESST)*, IEEE, Nov. 2015, pp. 62-65. doi: 10.1109/UNESST.2015.23.
 - [25] E. E. Başakın, Ö. Ekmekcioğlu, and M. Özger, "Drought prediction using hybrid soft-computing methods for semi-arid region," *Modeling Earth Systems and Environment*, vol. 7, no. 4, pp. 2363-2371, Nov. 2021, doi: 10.1007/s40808-020-01010-6.
 - [26] R. C. Deo and M. Şahin, "Application of the artificial neural network model for prediction of monthly standardized precipitation and evapotranspiration index using hydrometeorological parameters and climate indices in eastern Australia," *Atmospheric Research*, vol. 161-162, pp. 65-81, Jul. 2015, doi: 10.1016/j.atmosres.2015.03.018.

BIOGRAPHIES OF AUTHORS






Santoso Soekirno    is an expertise in the sensors and electronics area and actively lecturing the sensors and electronics instrumentation, he is also busy tutoring the students in completing their final projects, especially those related to the sensors and transducers. He was born in Jogjakarta on 4 April, 1961. He received his bachelor and master degrees from University of Indonesia and his doctor degree from the University of Besancon, France, in the field of the LC components with the dissertation title "frequency control parameters for oscillator sensor, a study on LC component". He can be contacted at email: santoso.s@sci.ui.ac.id.






Naufal Ananda    received bachelor of instrumentation engineering at Indonesian School of Meteorology, Climatology and Geophysics in 2019. He worked as calibration technician in Indonesian Meteorology, Climatology and Geophysics Agency since 2020. He is recently studying in Bandung Institute of Technology in Master Program of Instrumentation and Control. He can be contacted at email: naufal.ananda@bmkgo.id.






Haryas Subyantara Wicaksana    received bachelor of instrumentation engineering at Indonesian School of Meteorology, Climatology and Geophysics in 2019. He worked as calibration technician in Indonesian Meteorology, Climatology and Geophysics Agency since 2020. He is recently studying in Bandung Institute of Technology in Master Program of Instrumentation and Control. His research field comprises machine learning, measurement and calibration for meteorological and geophysics instrument. He can be contacted at email: haryas.wicaksana@bmkgo.id.






David Yulizar    holds a Bachelor of Instrumentation Engineering at School of Meteorology, Climatology, and Geophysics in Jakarta (2011-2016) and Master of Science (M.Sc.) in the Department of Physics, Faculty of Mathematics and Science, University of Indonesia (2021-2023). He currently works at the BMKG Region II Ciputat in the field of instrumentation and calibration. He can be contacted at email: david.yulizar@bmkgo.id.






Muhammad Agung Prabowo    earned his Associate Degree in Instrumentation in 2015 and later completed his Bachelor's degree in Applied Sciences in 2020, both from STMKG. Currently pursuing a Master's Degree in Physics with a specialization in Instrumentation at the University of Indonesia. Alongside his studies, he has been working at the Indonesian Agency for Meteorology, Climatology, and Geophysics (BMKG) since 2016 as technician, specializing in Instrumentation and Calibration of weather measurement instrumentation. With a keen interest in merging technology and science, Agung Prabowo contributes actively to the field. He can be contacted at email: muhammad.prabowo@bmkgo.id.



Suko Prayitno Adi    finished associate degree of geophysics in 1993 and bachelor degree of applied statistic at Universitas Terbuka UPBJJ – UT Jakarta in 1992. He continued his study in Sam Ratulangi Manado University, and reached master degree of regional development science in 1998. He received doctoral degree of public administration from Universitas Negeri Makasar (UNM). He has specialist research: applied meteorological and climatological data science in regional development, and implementation of tsunami risk and mitigation. Recently, he is a lecturer and dean of STMKG (Meteorological, Climatological and Geophysics Academy of Indonesia). He can be contacted at email: suko.prayitno.adi@stmkg.ac.id.



Bayu Santoso    obtained a Bachelor's degree in the field of instrumentation from the School of Meteorology, Climatology, and Geophysics in Jakarta, Indonesia. He currently works at BMKG Regional I in Medan as a laboratory calibration technician. Currently, he is pursuing a master's degree at the Bandung Institute of Technology, Indonesia, in the field of instrumentation and control. His research areas of interest include machine learning, the internet of things, and meteorological and geophysical instrumentation. He can be contacted at email: bayu.santoso@bmkgo.id.